Engineering Structures 74 (2014) 130–144

Contents lists available at ScienceDirect

Engineering Structures

journal homepage: www.elsevier.com/locate/engstruct

Numerical analysis of reinforced high strength concrete corbels

Rejane Martins Fernandes Canha [a,*], Daniel Alexander Kuchma [b], Mounir Khalil El Debs [c], Rafael Alves de Souza [d]

[a] Department of Civil Engineering, Federal University of Sergipe, Av. Marechal Rondon, s/n, Jardim Rosa Elze, São Cristóvão, SE 49100-000, Brazil
[b] Department of Civil and Environmental Engineering, University of Illinois at Urbana-Champaign, 205 North Mathews Ave., Urbana, IL 61801-2352, USA
[c] Department of Structural Engineering, School of Engineering of São Carlos of University of São Paulo, Av. Trabalhador Sãocarlense, 400, Pq Arnold Schimidt, São Carlos, SP 13566-590, Brazil
[d] Department of Civil Engineering, State University of Maringá, Av. Colombo, 5790, Jd. Universitário, Maringá, PR 87020-900, Brazil

ARTICLE INFO

Article history:
Received 24 September 2013
Revised 18 March 2014
Accepted 13 May 2014
Available online 6 June 2014

Keywords:
Corbel
Precast concrete
High strength concrete
Experimental results
Nonlinear analysis
Finite element method

ABSTRACT

This paper deals with comparisons of numerical results of reinforced high strength concrete corbels and experimental results obtained from the literature. The application of precast structures and high strength concrete have increased in the last years and taking into account the possibility of brittle failures using this solution, specific investigations are demanded to some structural details, as for example, corbels. It should be mentioned that brittle failures and complex regions are difficult to be analyzed by means of computational resources and for that reason it is argued if the available packages software are able to correctly describe the behavior of high strength concrete, specifically for corbels. In this way, the numerical simulations described in this paper have been conducted using the Finite element method. A parametric study was then carried out using the validated model to investigate the effect of the shear span-to-effective depth ratio, the main reinforcement rate and the compressive strength of concrete in the failure load and the contribution of secondary reinforcements. The main conclusions are: the numerical and experimental results showed a very close agreement, not only in the cracking and failure modes, but also in the load–deflection and load-reinforcement strain responses; there is a strong linear correlation of the failure load and shear span-to-effective depth ratio, the main reinforcement rate and the compressive strength of concrete; the horizontal secondary reinforcement improves the load capacity and could be considered in the design models; and the vertical secondary reinforcement only affects in the cracking distribution and ductility of the corbels.

1. Introduction

Corbels or brackets are very short cantilevers projecting from columns or walls that are usually used to support other parts of a structure, as for example, dapped-end beams. In precast concrete structures, reinforced concrete corbels are very common, especially by its facility of connection and speed during the construction process.

Schlaich et al. [1] have proposed the idea of subdividing a structure in "B-Regions" and "D-Regions", in order to introduce rational procedures for design reinforced/prestressed concrete structures. "B-Regions" follow the "Bernoulli Hypothesis", i.e., the hypothesis of linear deformations can be assumed through the whole cross section, since the beginning of the loading until the failure of the section. By another hand, "D-Regions" presents non-linear deformations throughout the cross section and the usual design procedures based on "Beam Theory" become inadequate and even unsafe whether applied. In these regions, usually some details of a structure, there is a complex stress state mainly generated by shear deformations. As examples of "D-Regions" the following parts of a structure may be mentioned: pile caps, footings, deep beams, corbels, dapped end beams and prestressed anchorages.

Generally, "D-Regions" are produced by static (loadings) and/or geometric perturbations, and the length of these discontinuity regions may be found using the Saint Venant Principle, i.e., the zones of dissipation of perturbations are usually defined based on the height of the member. In this way, corbels may be considered discontinuity regions ("D Regions") as a whole, and the application of beam theory is not recommended. For designing corbels, tools like Strut-and-Tie, Shear-Friction models and finite element analysis are usually necessary in order to better understand the mechanisms of resistance of the element.

* Corresponding author. Address: R. João Vitor de Matos, 10, apt. 602, Farolândia, Aracaju, SE, Brazil. Tel.: +55 79 8868 6167.
E-mail addresses: rejane_canha@yahoo.com.br (R.M.F. Canha), kuchma@illinois.edu (D.A. Kuchma), mkdebs@sc.usp.br (M.K. El Debs), rsouza@uem.br (R.A. de Souza).

http://dx.doi.org/10.1016/j.engstruct.2014.05.014
0141-0296/

Although during the past decades many experimental researches on corbels have been carried out and new theoretical models have been also proposed, empirical approaches and common detailing practices are still used due to the fact that there is not a convergence in the design models, as it can be noted in the codes such as ACI Committee 318/08 [2], PCI Design Handbook 2010 [3], and Eurocode 2/04 [4]. As example, the ACI Committee 318/08 [2] recommends that the corbel-column interface should be designed to resist simultaneously the vertical and horizontal loads and the moment caused by these loads, adopting the largest reinforcement calculated by a Shear-Friction or a flexural model both combined with the horizontal tensile force, besides provisions for secondary reinforcement. In the PCI Design Handbook 2010 [3], there is a Shear-Friction model accounting for the main and secondary reinforcements and a Strut-and-Tie model considering only the main reinforcement. The Eurocode 2/04 [4] recommends a Strut-and-Tie method with a main and a secondary tie and to limit the slope of the main strut.

By another hand, the numerical analysis validated with experimental results can aid in the correct application of the available models, solving questions referred to some controversial parameters used in these models, such as: the effective stress in the strut and bearing plate of the Strut-and-Tie model, the effect of the shear span-to-effective depth ratio in the failure mode and the contribution of secondary reinforcements. Regarding numerical analysis of corbels, there are few publications, deserving mention the papers published by Strauss et al. [5], Gao and Zhang [6], Souza [7], Rezaei et al. [8], and Syroka et al. [9], but none of them emphasizes the high strength concrete.

For having a realistic analysis of corbels, the constitutive models available in the software packages should provide at least nonlinear constitutive relationships for the materials and some additional effects like tension stiffening and compression softening. In this way, the mechanisms of failure may be analyzed expecting relatively good precision, especially when using high strength concrete.

Despite the fact that high strength concrete has brittle behavior when compared to normal strength concrete, its utilization has become a tendency in precast concrete structures. This fact is mainly due to its high durability and the possibility of decreasing the elements dimensions. As mentioned, the failure of high strength concrete by crushing is brittle and there are still some doubts regarding the design of corbels using this material.

In this paper, some experimental results of high strength concrete corbels selected from literature (Yong et al. [10], Yong and Balaguru [11], Fattuhi and Hughes [12–14], Fattuhi [15], Selim et al. [16], Powel and Foster [17], Foster et al. [18], Reis and Torres [19], Torres et al. [20], Naegeli [21], Torres [22], Fernandes [23], Bourget et al. [24], Campione et al. [25,26]) have been compared with numerical results generated using the nonlinear finite element program ATENA. In order to check the performance of the selected software package, the following items were investigated: cracking, failure load and failure mode, concrete and reinforcement principal strains, load-deformation response and load-reinforcement strain response.

2. Experimental results

Experimental data of hundred corbels available in the references mentioned before were selected to be analyzed. The specimens have been selected according to the following properties:

- Symmetrical corbels in order to avoid bending effects.
- Rectangular or chamfer shaped corbels with external height h_{ext} at least equal to half of height h (see Fig. 1).
- Failure mode described and not due to local effects (column, external edge or anchorage failures).
- Concrete strength equal to or larger than about 40 MPa (usual starting value for considering concrete as of high strength).
- Reinforcement placed in the horizontal and vertical directions.

An extensive number of variable parameters was included in this study, such as: shear span-to-effective depth ratio (a/d), corbel width (b), corbel height (h), corbel length (c), loading plate width (w_p), main reinforcement rate (ρ_{sm}), horizontal and vertical secondary reinforcements rates (ρ_{shs} and ρ_{svs}), vertical and horizontal load ratio (H/V), yielding strength of steel (f_y) and compressive strength of concrete (f_c).

Normally, the horizontal secondary reinforcement (A_{shs}) should be distributed along two thirds of the effective depth of the corbel ($2d/3$). In this way, for the calculation of this reinforcement (A_{shs}) and the corresponding reinforcement rate (ρ_{shs}), only the stirrups positioned in this branch were considered. On the other hand, for the determination of the vertical secondary reinforcement (A_{svs}) and the corresponding reinforcement rate (ρ_{svs}), only the vertical stirrups located along the shear span (a) were taken into account.

Fig. 1 illustrates the variables considered in the corbels and Table 1 presents the values interval of these parameters from the selected specimens.

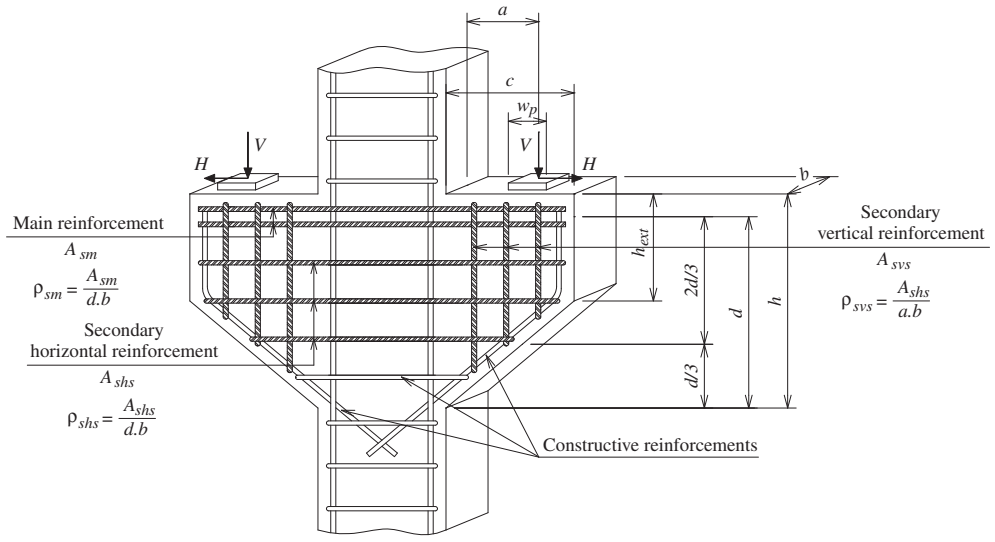

Fig. 1. Dimensions and reinforcements used in reinforced concrete corbels.

Table 1
Experimental parameters of the corbels.

Experimental research	Initials	a/d	b (mm)	h (mm)	c (mm)	w_p (mm)	ρ_{sm} (%)	ρ_{shs} (%)	ρ_{svs} (%)	H/V	f_y (MPa)	f_c (MPa)
Yong et al. [10], Yong and Balaguru [11]	YO	0.25–0.75	254	406 and 407	254	90	0.43–2.13	0.31–1.14	0	0 and 0.2	383–621	39–82
Fattuhi and Hughes [12], [13], [14], Fattuhi [15]	FA	0.41–1.04	150 and 152	150–246	200 and 300	50[a]	0.49–1.17	0–1.61	0	0	452–558	40–73
Selim et al. [16], Powel and Foster [17], Foster et al. [18]	FO	0.30–1.00	125 and 150	600–800	300–550	100–150	0.57–4.93	0–0.70	0	0	360–495	45–105
Reis and Torres [19], Torres et al. [20]	RT	0.37	180	653	338	150	0.43	0.29 and 0.43	0	0	570	47–50
Naegeli [21]	NA	0.37	120	450	225	100	0.38	0–0.77	0	0	614	37–84
Torres [22]	TO	0.50	150	350	250	100	1.09	0–0.28	0–0.52	0	486–760	50–79
Fernandes [23]	FE	0.57–0.95	120	120	120 and 140	50	0.63–1.57	0.44 and 0.62	0.46–1.09	0	525–750	74–94
Bourget et al. [24]	BO	0.25–0.39	150	360	250	50	0.20–0.92	0.11–1.27	0	0	500–550	70–132
Campione et al. [25,26]	CA	0.79–0.93	160	160	190	50[a]	0.70–1.80	0–0.76	0	0	445–570	49–79

[a] This value was adopted because it was not reported in the reference.

3. Aspects of the numerical modeling

Fig. 2 illustrates the upside down test arrangement, similar for all experimental researches, and the corresponding numerical model arrangement. The displacement control during the load application was used in only some tests. For the numerical models, the loading was applied in a similar way of these tests, i.e., as a uniform vertical displacement at the bottom of the column considering also the displacement control, which is a more numerically stable approach for capturing the post peak behavior. The load corresponding to this applied displacement is calculated during the processing. Also, a vertical roller support was added in the middle node at the top of the steel plate. Among the references included in this work, Yong et al. [10] and Yong and Balaguru [11] were the only ones that analyzed the effect of vertical and horizontal loads ratio (H/V) in the behavior of the corbels. For the eight specimens of these authors that had an applied horizontal load, the roller support was sloped to provide horizontal and vertical reactions.

To take advantage of the symmetry of the corbels and save processing time, only one half of each model was constructed and the horizontal freedom degree of the nodes of the column medium line was restricted by applying horizontal roller supports.

In order to reduce some stress concentrations due concentrated loads and avoid a local failure in the elements near the loading point, linear elastic steel plates were added to the model subdivided in three layers with gradual increase of modulus of elasticity ($E_c + E_s/3$; $E_c + 2E_s/3$; $E_c + E_s$) from the concrete interface to the loading point, as Fig. 2 shows.

The material model SBETA is used in ATENA to model the nonlinear behavior of concrete. This model is based on a plane stress state and uses smeared material properties, including the development of cracks. In such models, the smeared properties are only valid within a certain volume of material. This volume should be properly represented by the element size chosen for the finite element mesh. The material model SBETA includes the important effects of concrete behavior, such as: non-linear behavior in compression, including hardening and softening; fracture of concrete in tension based on the nonlinear fracture mechanics; biaxial strength failure criterion; reduction of compressive strength after cracking; tension stiffening effect; reduction of the shear stiffness after cracking; fixed crack and rotated crack models. More information regarding ATENA may be obtained in Cervenka and Cervenka [27,28].

The concrete of the corbels including the columns was meshed only using one macro-element. The macro-element in ATENA represents a homogeneous region with the same properties. As the third out-of-plane dimension little affects the corbel behavior, only the two-dimensional analysis was considered. The preliminary simulations carried out in the corbels in order to evaluate the best parameters of the concrete constitutive model led to the values and options described in of Table 2. As the average concrete properties such as the modulus of elasticity E_c, the tensile strength f_t and compressive strain at compressive strength of the concrete in the uniaxial direction ε_c were not reported in the most of references, the values of Table 2, calculated in function of the average compression strength f_c and applicable to high strength concrete, were used.

Reinforcement can be modeled in two different ways: smeared and discrete. Smeared rebar may be placed in each element based on a reinforcement ratio in any direction desired. Another approach is to add discrete rebar lines modeled by truss elements between any two points of the model, which are not necessarily the nodes of the concrete. For both cases, the following stress–strain relationships may be used to model the uniaxial stress state of the reinforcement: bilinear, with or without hardening, multi-linear and cycling model.

Due to the simplicity of the preprocessor available in ATENA, all reinforcements were represented by discrete rebar elements,

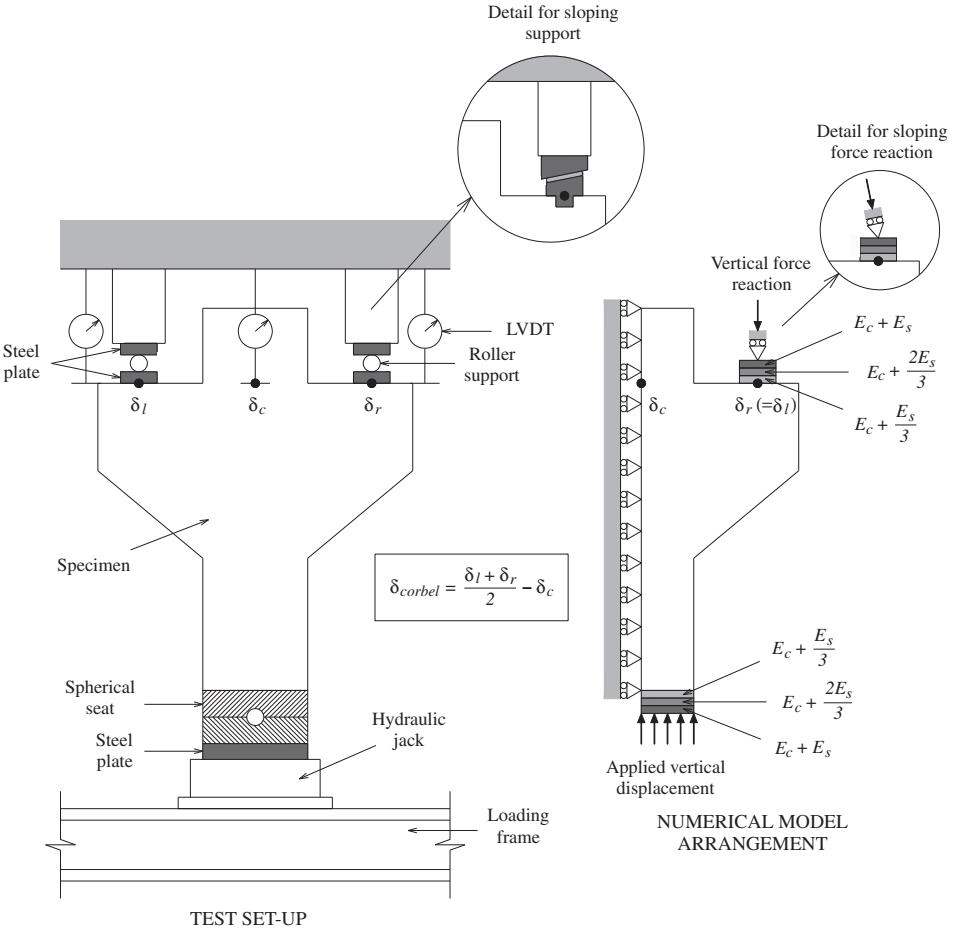

Fig. 2. Test set-up and arrangements for the numerical models.

Table 2
Concrete parameters selected in ATENA.

Parameter:	Formula:
Initial elastic modulus	$E_c = 3320\sqrt{f_c} + 6900$ [MPa] [a] with f_c in MPa
Poisson's ratio	$\mu = 0.2$[d]
Strength tensile	$f_t = 0.33\sqrt{f_c}$ [MPa] [b] with f_c in MPa
Type of tension softening	Exponential, based on G_f [d]
Fracture energy (MN/m)	$G_f = 0.000025 f_t$[MN/m] [d] with f_t in MPa
Compressive strain at compressive strength in the uniaxial compressive test	$\varepsilon_c = \frac{f_c}{E_c}\left(\frac{0.8+\frac{f_c}{17}}{0.8+\frac{f_c}{17}-1}\right)$ [c] with f_c and E_c in MPa
Compressive strength reduction factor of cracked concrete	$c = 0.8$[d]
Type of compression softening	Crush band[d]
Crack model	Fixed[d]
Critical compressive displacement	$w_d = -0.5$ mm[d]
Shear retention factor	Variable[d]
Tension–compression interaction	Linear[d]

[a] ACI Committee 363/93 [32].
[b] Vecchio and Collins [33].
[c] Thorenfeldt et al. [34].
[d] Default.

including the column reinforcements. The elastic-perfectly plastic behavior was considered and the rebar elements were assumed perfectly bonded to the concrete. The default value for the steel elasticity modulus of E_s = 200 GPa was adopted. For the nonlinear solution, the full Newton–Rhapson Method was used, in which the stiffness matrix is updated at each iteration.

In ATENA, the concept of the failure band based on "crack band theory" of Bazant and Oh [29] is used for both tension and compression failures in order to eliminate the element size effect and the element orientation effect. These are two deficiencies that may occur when applying the finite element model and more information of these problems can be found in Rots et al. [30] and Feenstra and Borst [31].

In order to analyze if different results may be produced in function of the smeared approach, preliminary numerical simulations were carried out in some corbels. For corbels in full scale, the element sizes considered were 25 mm (fine mesh), 50 mm (medium mesh) and 75 mm (coarse mesh). For the reduced scale corbels, element sizes

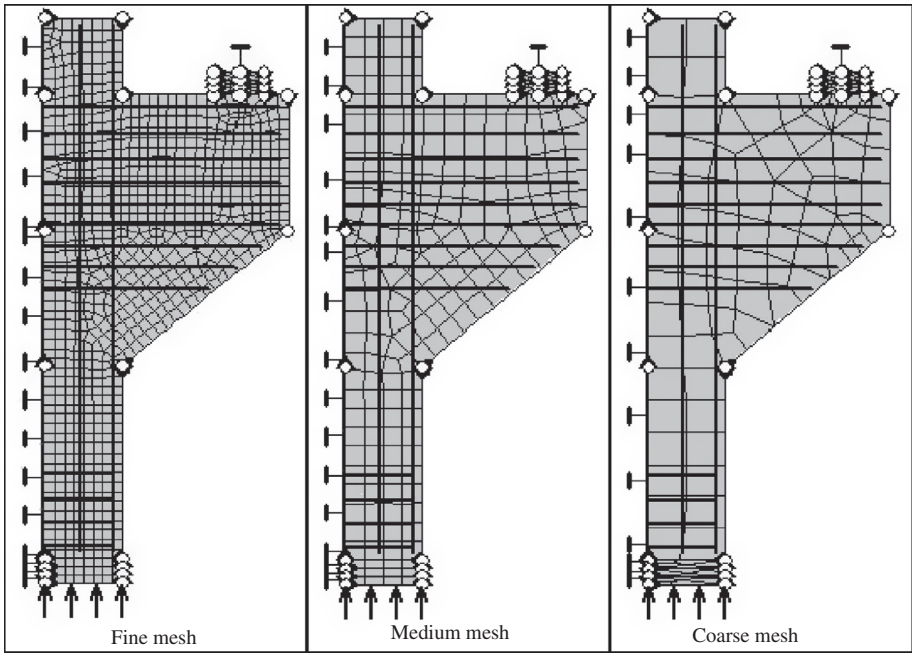

Fig. 3. Models investigated with three different mesh sizes.

of 12.5 mm (fine mesh), 25 mm (medium mesh) and 37.5 mm (coarse mesh) were considered. Fig. 3 shows three mesh sizes of a corbel with the reinforcement bars and the boundary conditions.

Fig. 4 shows the load–deflection and load-reinforcement strain behavior for two corbels. Some aspects regarding the three mesh sizes should be highlighted. All theoretical curves were reasonably close to each other and to the experimental ones. The mesh size did not affect significantly the behavior of the corbel, but the numerical curves were a little bit stiffer than the corresponding experimental curves for some corbels. This confirms the validation of the smeared approach and the reduction of the element size and element orientation effects used in ATENA. However, the medium size mesh was used for the next numerical simulations, in order to avoid an excessive computational effort and loss of precision in characterization of the cracking pattern.

4. Numerical results

4.1. Failure load and modes

Although there is a diversity of names for the failure modes according to the technical literature, basically four groups of failure modes can be highlighted:

- Flexural or tension failure (T): the flexural failure, also designated of tension failure by Foster et al. [18], is characterized by wide openings of flexural cracks which propagate vertically near the interface column-corbel and occurs after an extensive yielding of the tension reinforcement, accompanied by local concrete crushing at the internal bottom corner of the corbel. It can also be noted diagonal shear cracks, in this failure, that remain with small openings, named as flexure–shear failure by Fattuhi and Hughes [14]. This is the ideal situation for design, since that this failure is gradual and rather ductile, allowing the repair before the collapse of the structure. This failure usually is observed for low values of the main reinforcement rates (ρ_{sm}) times the corresponding yielding stress (f_{ym}) or large shear span to effective depth ratios (a/d), as mentioned by Powell and Foster [17].
- Compression failure (C): this type of failure can be associated to a flexural compression (FC) or a diagonal splitting (DS). The flexural compression, also named of beam shear by Mattock et al. [35] and Yong et al. [10], inclined shear by Fattuhi and Hughes [12], shear by Fattuhi [36] and Hagberg [37], is characterized by widening of multiple diagonal shear cracks along the diagonal region between loading plate and the internal bottom corner of the corbel, followed by the concrete crushing at this area. This failure is abrupt and the flexural cracks remain with small

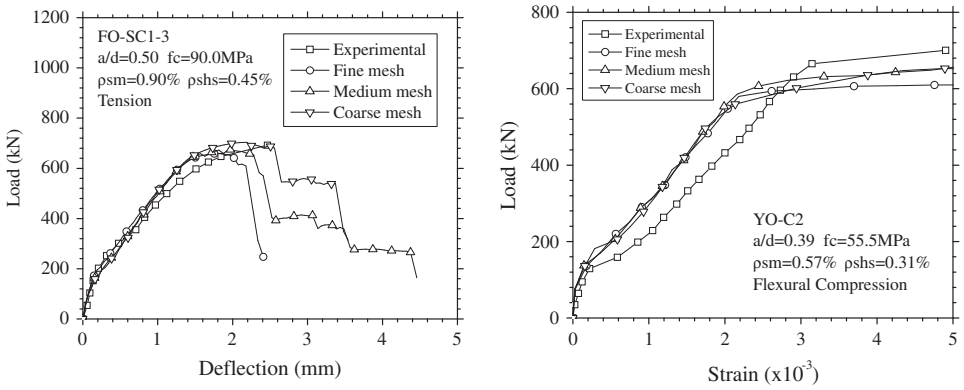

Fig. 4. Comparison of results of models with three different mesh sizes.

Table 3
Comparisons regarding experimental and numerical results.

Specimen	a/d	Failure load		Load efficiency factor	Experimental failure mode		Numerical failure mode
		Vu,exp (kN)	*Vu,num* (kN)	$\frac{V_{u,exp}}{V_{u,num}}$	According to the data of references	Based on yielding or not of main reinforcement	
YO-B1	0.39	778	562	1.38	C–FC	T	T
YO-B2	0.39	667	560	1.19	C–FC	T	T
YO-C1	0.39	796	711	1.12	C–FC	T	T
YO-C2	0.39	836	682	1.23	C–FC	T	T
YO-D1	0.39	701	641	1.09	C–FC	T	T
YO-D2	0.39	801	696	1.15	C–FC	T	T
YO-E1	0.25	712	711	1.00	C–FC	T	T
YO-E2	0.25	801	715	1.12	C–FC	T	T
YO-E3	0.25	1079	1575	0.69	C–FC	T	T
YO-F1	0.50	912	633	1.44	C–FC	T	T
YO-F2	0.50	845	903	0.94	C–FC	T	T
YO-G1	0.75	337	569	0.59	C–FC	C	C[a]
YO-G2	0.75	411	596	0.69	C–FC	T	C[a]
YO-G3	0.75	556	701	0.79	C–FC	C	C
FA-T1	0.74	93	102	0.91	C–DS	C	C[a]
FA-T2	0.74	146	152	0.96	C–FC	C	C[a]
FA-T6	0.74	136	155	0.88	C–DS	T	T
FA-T7	0.74	157	165	0.95	C–FC	C	C[a]
FA-T8	0.74	188	184	1.02	C–FC	T	C[a]
FA-T9	0.74	153	176	0.87	C–FC	C	C[a]
FA-C1	1.04	80	80	1.00	C–DS	C	C[a]
FA-C21	0.44	114	115	0.99	S	T	T
FA-C22	0.74	82	75	1.09	T	T	T
FA-C23	1.04	47	56	0.84	C–DS	T	T
FA-C24	0.44	145	183	0.79	S	C	T
FA-C25	0.54	151	183	0.83	S	T	C[a]
FA-C26	1.04	90	96	0.94	C–DS	C	C[a]
FA-116	0.76	115	101	1.14	C–DS	C	T
FA-117	0.80	153	139	1.10	C–DS	C	T
FO-SA1	0.34	1200	1298	0.92	B	C	C
FO-SA3	0.34	860	722	1.19	T	T	T
FO-SA4	0.34	1500	1242	1.21	C–FC	C	C
FO-SB1	0.34	1000	910	1.10	B	C	C
FO-SC1-2	0.50	950	986	0.96	C–DS	C	C
FO-SC1-3	0.50	700	675	1.04	T	T	T
FO-SC1-4	0.55	470	509	0.92	T	T	T
FO-SC2-1	0.50	980	881	1.11	C–FC	C	C
FO-SC2-2	0.50	700	807	0.87	C–DS	C	C
FO-SC2-3	0.50	580	618	0.94	T	T	T
FO-SC2-4	0.50	490	521	0.94	C–DS	T	T
FO-SD1	0.50	1000	1014	0.99	C–FC	C	C
FO-SD2	0.50	1000	900	1.11	C–FC	C	C
FO-PA1	0.60	550	721	0.76	C–DS	C	C
FO-PA2	0.60	800	722	1.11	C–DS	C	C
FO-PB1	0.60	1180	1347	0.88	C–DS	C	C
FO-PB2	0.60	1150	1335	0.86	C–FC	C	C
FO-PC1	0.30	650	708	0.92	C–DS	C	T
FO-PC2	0.30	1040	919	1.13	C–FC	C	T
FO-PD2	0.40	960	1158	0.83	C–FC	C	C
FO-PE1	1.00	680	509	1.34	C–DS	C	C
FO-PE2	1.00	710	528	1.34	C–FC	C	C
FO-PF1	0.30	750	817	0.92	T	T	T
FO-PF2	0.30	1050	1110	0.95	T	T	T
FO-PG1	0.60	674	572	1.18	C–FC	C	C
FO-PG2	0.60	1050	929	1.13	C–FC	C	C
RT-C11	0.37	820	825	0.99	C–DS	T	T
RT-C12	0.37	950	928	1.02	C–DS	C	T
NA-SP2	0.37	235	273	0.86	C–FC	T	T
NA-SP4	0.37	220	254	0.87	C–FC	C	T
NA-SP5	0.37	275	315	0.87	C–FC	T	T
NA-SP6	0.37	275	306	0.90	C–FC	T	T
NA-SP8	0.37	315	293	1.08	C–FC	T	T
NA-SP9	0.37	295	306	0.96	C–FC	T	T
NA-SP10	0.37	450	419	1.07	C–FC	T	T
NA-SP11	0.37	425	352	1.21	C–FC	T	T
NA-SP12	0.37	320	274	1.17	C–FC	T	T
NA-SP13	0.37	315	327	0.96	C–FC	T	T
NA-SP14	0.37	370	367	1.01	C–FC	T	C[a]
TO-CH0V0	0.50	500	417	1.20	C–DS	T	T

(*continued on next page*)

Table 3 (*continued*)

Specimen	a/d	Failure load		Load efficiency factor	Experimental failure mode		Numerical failure mode
		Vu,exp (kN)	*Vu,num* (kN)	$\frac{V_{u,exp}}{V_{u,num}}$	According to the data of references	Based on yielding or not of main reinforcement	
TO-CH5V5	0.50	625	468	1.34	C–DS	T	T
TO-CH5V0	0.50	535	451	1.19	C–DS	T	T
TO-CH0V5	0.50	483	442	1.09	C–DS	T	T
TO-CH4V4	0.50	540	448	1.21	C–DS	T	T
TO-CH4V0	0.50	580	473	1.23	C–DS	T	T
TO-CH6V0	0.50	598	467	1.28	C–DS	T	C[a]
TO-CH4V4*	0.50	395	399	0.99	C–DS	T	T
FE-CS5-4A	0.57	150	142	1.06	C–FC	T	T
FE-CD6-4A	0.57	180	159	1.13	C–FC	T	T
FE-CS6-4A	0.57	160	158	1.01	C–FC	T	T
FE-CS8-5A	0.57	200	223	0.90	B	T	T
FE-CD5-4B	0.76	110	108	1.02	C–FC	T	T
FE-CD6-4B	0.76	124	122	1.02	C–FC	T	T
FE-CS6-4B	0.76	123	121	1.02	C–FC	T	T
FE-CS8-5B	0.76	175	174	1.01	B	T	T
FE-CS5-4C	0.95	100	86	1.16	T	T	T
FE-CD6-4C	0.95	106	95	1.12	C–FC	T	T
FE-CS6-4C	0.95	120	97	1.24	C–FC	T	T
FE-CS8-5C	0.95	156	140	1.11	C–FC	T	T
BO-C1-80	0.37	282	217	1.30	T	T	T
BO-C2-80	0.37	448	402	1.11	T	T	T
BO-C3-80	0.25	807	884	0.91	T	T	T
BO-C1-100	0.25	980	1073	0.91	T	T	T
BO-C2-100	0.37	550	433	1.27	T	T	T
BO-C1-120	0.25	1117	1133	0.99	C–FC	T	T
BO-C2-120	0.39	997	920	1.08	C–FC	T	T
CA-MI-2ϕ10	0.93	79	87	0.91	C–FC	T	T
CA-MI-2ϕ10 + 4ϕ6	0.93	97	106	0.92	C–FC	T	T
CA-MII-2ϕ10	0.79	119	106	1.12	C–FC	T	T
CA-MII-2ϕ16	0.79	165	218	0.76	C–FC	C	C
CA-MII-2ϕ10 + 4ϕ6	0.79	189	137	1.38	C–FC	T	T
Average				1.03	Standard deviation (%)		16.4
Variation coefficient (%)				15.9	Coefficient of determination R^2		0.914

T: Tension failure.

C : Compression failure { FC : Flexure – Compression failure; DS : Diagonal Splitting failure

S: Shear failure.

SE : Secondary failure { A : Anchorage failure of the main reinforcement; B : Bearing failure of the concrete under the load plate

[a] Main reinforcement close to yielding.

openings. The diagonal splitting was first reported by Kriz and Raths [38]. This failure, also designated of diagonal tension failure by Mattock et al. [35], is similar to the flexural compression failure, however presenting the difference of a single wide diagonal crack instead of multiple cracks pattern, leading then to a more brittle collapse than the flexural compression failure. According to Kriz and Raths [38], the diagonal splitting does not occur with the use of adequate secondary horizontal stirrups, which modify this failure to a more ductile flexural compression failure. Although the compression failure is characterized only if the main tension reinforcement has not yielded, in the opinion of the present authors, a third intermediate compression failure could be specified, denominated of compression–tension (C–T), with a predominant compression and a secondary tension. In this failure mode, the main reinforcement yields few instants before or practically at the same time of the compression failure. For this failure mode, the maximum capacities of steel and concrete are demanded as in the tension failure, with the difference that the compression–tension mode is brittle as in the compression failure by flexure–compression or diagonal splitting.

- Shear failure (S): this failure, also known as shear by Somerville [39], constrained shear or sliding shear by Fattuhi and Hughes [12], occurs with the development of a series of inclined cracks along the column-corbel interface. The connection of these multiple inclined cracks forms a weakened plane, followed by the relative slip between the corbel and the column. This kind of failure is more common in corbels with low values of shear span to effective depth ratio (a/d).
- Secondary failure (SE): according to Powell and Foster [17], this failure is characterized by the anchorage failure of the main reinforcement (A) or the bearing failure of the concrete under the load plate (B). Both failures can be avoided with an appropriate design and building of the corbel.

Considering the difficulty of establish the directions and magnitude of opening in the cracking pattern and a fracture plane, for a numerical analysis, it is more convenient to classify the failure mode by the occurrence or not of the yielding of the main tension reinforcement, as the criterion adopted by Foster et al. [18]. The compression failure (C) is described by concrete crushing or diagonal splitting, both identified by the crack pattern, only if the main tension reinforcement has not yielded. The tension failure (T) corresponds to a corbel failure by any mode after the yielding of the main tension reinforcement. Therefore, the failure modes of the numerical models were classified according to this criterion.

It should be highlighted that for some corbels of some references, as in Fattuhi and Hughes [12–14], Fattuhi [15], Campione et al. [25,26], due to the absence of measurements in the main reinforcement, the occurrence or not of the yielding of this one in the

tested specimens was based on comments of the authors, pictures of the cracking pattern and the load–displacement behavior. Table 3 shows the experimental and numerical failure loads and modes.

Despite the fact that some parameters, such as the width plate, the position of the reinforcements, the yield stress and others, needed to be adopted or approached for some corbels, once they were not described in the references, the experimental failure mode by tension or by compression was well captured in the numerical analysis for almost all corbels. This was primarily noted for the corbels with a more complete characterization.

The load efficiency factor can defined by the ratio between the experimental ultimate load and the corresponding numerical value. Generally, this load efficiency factor was close to one, with the average factor larger than one, which is the desirable value for a safe analysis. The standard deviation was 16.4% and the variation coefficient referred to the load efficiency factor was 15.9%. This value seems to be rather reasonable for a theoretical analysis, considering that there are several parameters and variations of these ones that directly affect the behavior of each corbel.

Although there were some differences in the ultimate loads, these variations for practical issues are small. Besides, analyzing the coefficient of determination R^2 shown in Table 3, which indicates how closely values obtained from fitting models match the experimental results, it can be concluded that the numerical simulation provided a very good prediction of the experimental failure load.

4.2. Load versus deflection response

The curve load–displacement, including the early stages of loading, the decrease of stiffness after the linear-elastic regime, the existence or not of a plateau, the maximum load and the post-peak behavior until the complete degeneration of a corbel can be used in order to characterize its general behavior. The relative deflection is the most representative displacement and it is calculated as the difference between the average displacement of both corbels, taken from the central point of the steel plate bottoms, and the displacement of a point in the middle of the column (Fig. 2). In the case of the numerical models, taking into account the symmetry, the left and right displacements (δ_l and δ_r) of the left and right corbels, respectively, will be the same.

It should be highlighted that only few authors characterized the complete behavior of the tested corbels, including the load–deflection response, the load–strain of reinforcement curve and the cracking pattern. Among the available experimental results, the most detailed report of the tested specimens are the ones described by Selim et al. [16], Powel and Foster [17] and Foster et al. [18].

To validate the numerical simulation, some corbels of these authors and Naegeli [21] were selected for evaluation of the load–deflection behavior, and other corbels of Yong et al. [10], Yong and Balaguru [11], Torres [22] and Bourget et al. [24] were used for comparison of the load–strain of reinforcement response. The load–deflection responses for the selected corbels with different characteristics and failure modes are illustrated in Fig. 5. However, it should be highlighted that the experimental post-peak of the load–deflection response of these corbels was not presented in the original references, not allowing the comparison with the numerical curves. The theoretical curves were reasonably close to the experimental ones, but the numerical curves were a little bit stiffer than the corresponding experimental curves for some corbels.

4.3. Load versus reinforcement strain response

Fig. 6 shows the load-reinforcement strain behavior for the corbels tested by Torres [22] and Bourget et al. [24].

It should be highlighted that the experimental post-peak behavior of the reinforcements of all corbels was not shown in the original references, not allowing the comparison with the numerical curves.

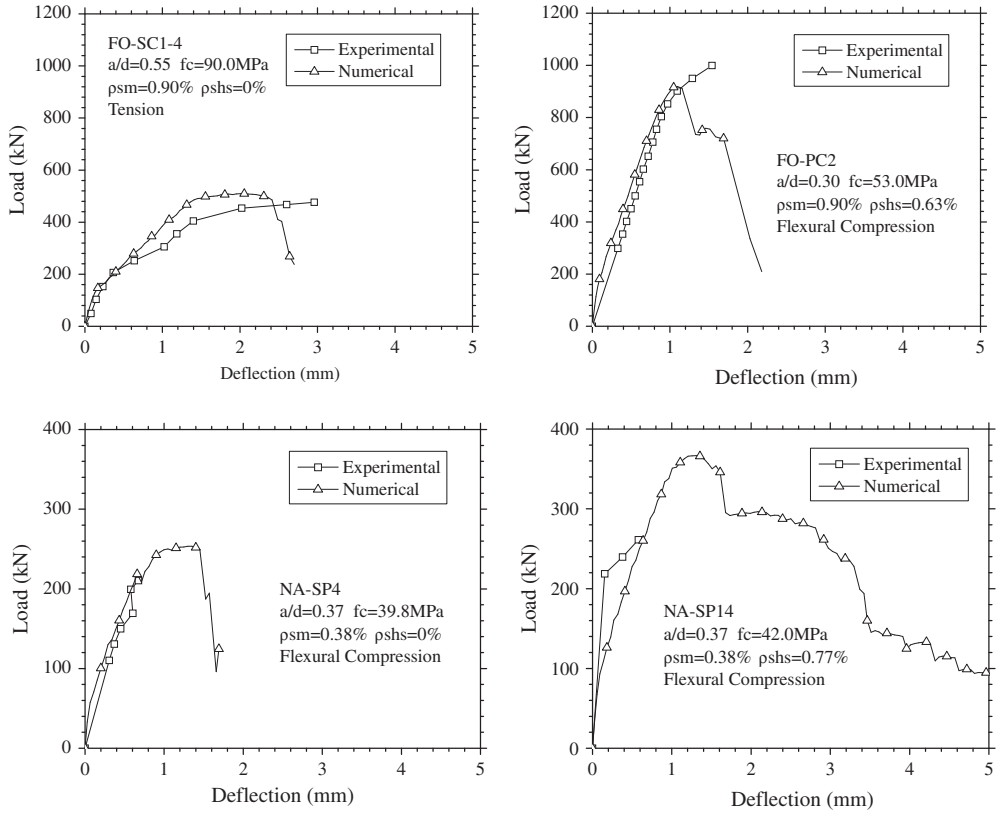

Fig. 5. Load–deflection response for some investigated corbels.

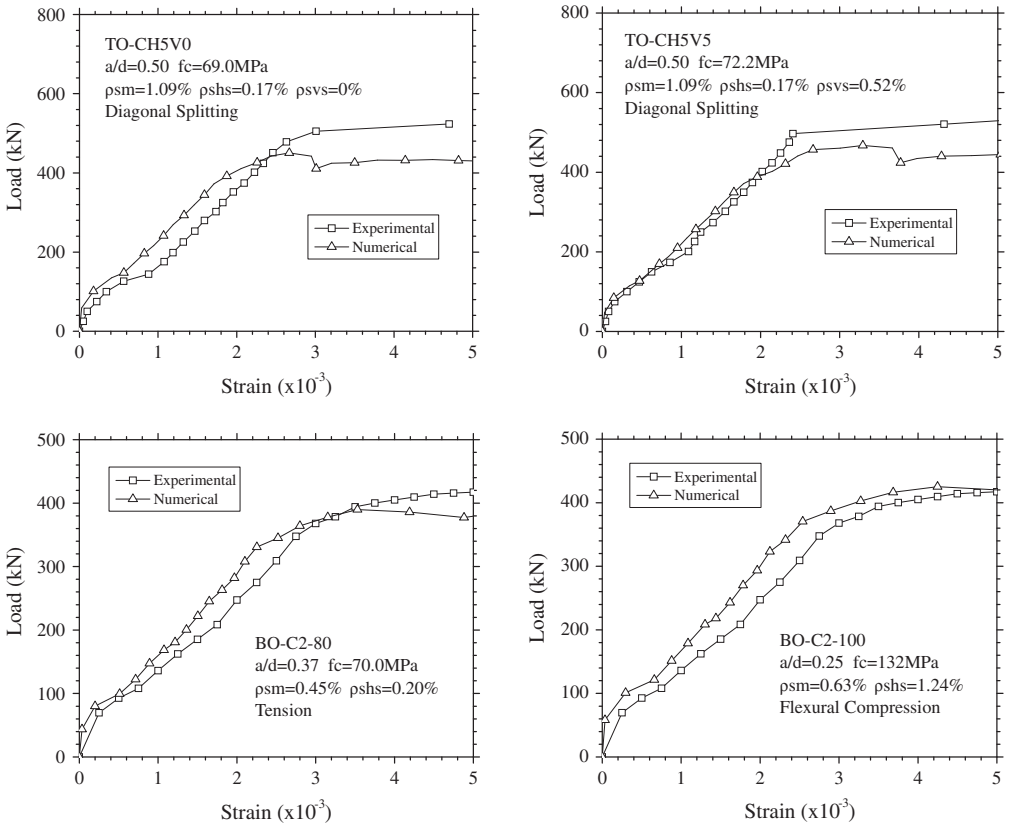

Fig. 6. Load–reinforcement strain response for some investigated corbels.

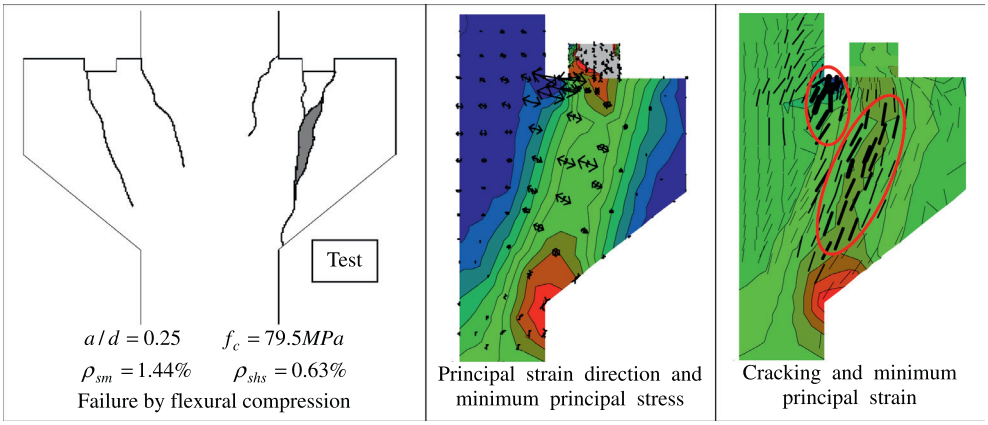

Fig. 7. Cracking, minimum principal stress and strain at failure load of corbel YO-E3.

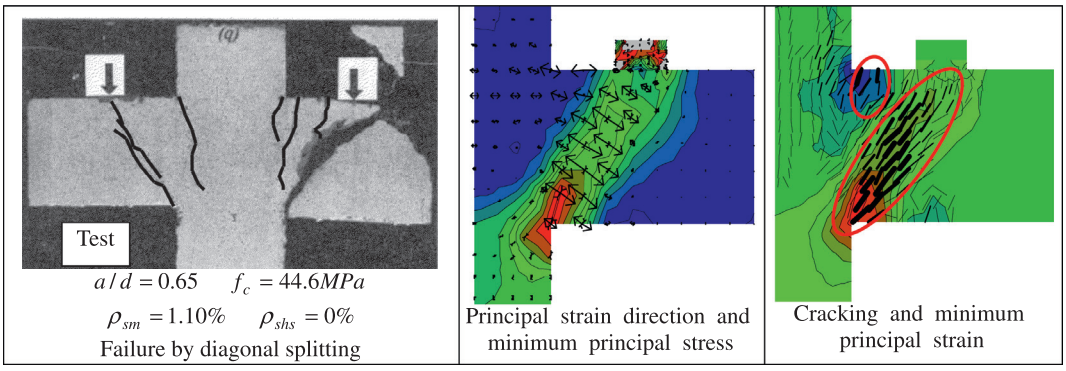

Fig. 8. Cracking, minimum principal stress and strain at failure load of corbel FA-T6.

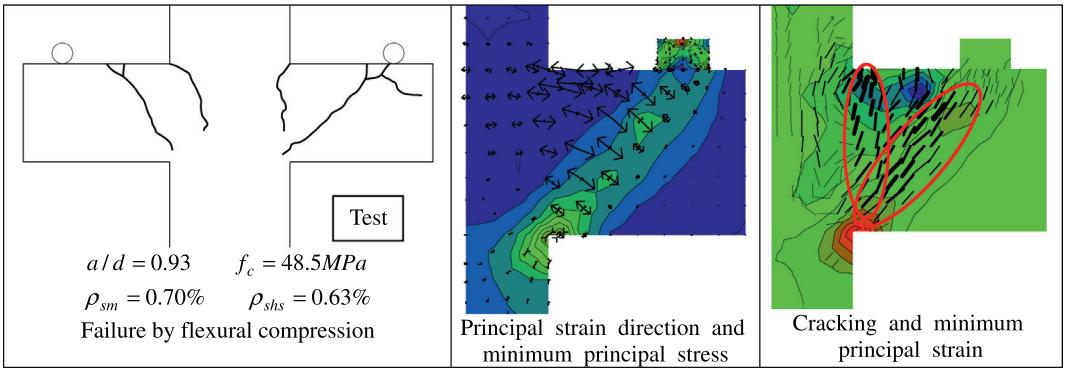

Fig. 9. Cracking, minimum principal stress and strain at failure load of corbel CA-MI-2ϕ10.

The numerical curves of all corbels were a little bit stiffer than the corresponding experimental ones for some corbels. The numerical curves were reasonably close to the experimental curves. Considering the variability of parameters, not only to the experimental specimens, but also to the numerical models, the response of the specimens was well captured by ATENA.

4.4. Cracking pattern, stress and strain

In order to validate this numerical analysis in all aspects, three corbels of different authors were selected to illustrate the cracking, minimum principal stress and strain. Figs. 7–9 show the cracking, minimum principal stress and strain patterns of corbels YO-E3 (Yong and Balaguru [11]), FA-T6 (Fattuhi and Hughes [14]) and CA-MI-2ϕ10 (Campione et al. [25], Campione et al. [26]), respectively, which were chosen with different characteristics.

The numerical simulation provided a good response related to the cracking, minimum principal stress and strain for the analyzed corbels. For corbel YO-E3, which has a lower shear span-to-effective depth ratio *a/d*, a steep compression stresses and strains fields from the plate to the lower corner of the corbel-column interface and a smeared cracking in the upper region of the corbel-column interface were observed as the experimental cracking pattern.

For corbel FA-T6, the diagonal splitting of the concrete the smeared cracking in the upper region of the corbel-column interface was verified in the numerical specimen. For corbel CA-MI-2ϕ 10, both the diagonal cracking and the smeared cracking in the corbel-column interface visualized in the tested specimen was observed in the numerical specimen.

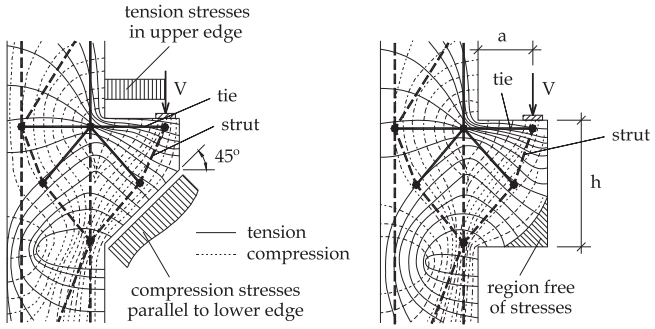

Fig. 10. Strut-and-Tie Model for chamfer shaped and rectangular corbels (adapted from Leonhardt and Mönnig [40]).

4.5. Association of the corbel behavior with the Strut-and-Tie and Shear-Friction Models

The two mechanisms that govern the behavior of reinforced concrete corbels are originated from the Strut-and-Tie Model (Fig. 10) and Shear-Friction Model (Fig. 11), where one is more predominant than the other depending on the shear span-to-effective depth ratio *a/d*.

Strut-and-Tie Model has as principal idea the substitution of the real structure by a truss form resistant structure, which simplifies the original problem in a systematical way, as shown in Fig. 10. In these hypothetical trusses, the compressive concrete elements, which represent the compression fields of the original structure, are denominated struts, while the tensile steel elements, which represent the tension fields, are referred as ties. The points of intersection between struts and ties, i.e., the points where there is a distribution of forces, are referred as "nodal regions". The stress level established in the nodal regions, as well as in the struts, should be limited to a certain value of the compressive concrete strength, in a way of avoiding cracks or premature failure. However, there is a great difficult for establishing this level of stress, taking into account the diversity of possibilities regarding the geometry of nodal zones, as well as struts.

The Shear-Friction Model is a semi-empirical approach which supposes that a crack can form along the corbel-column interface,

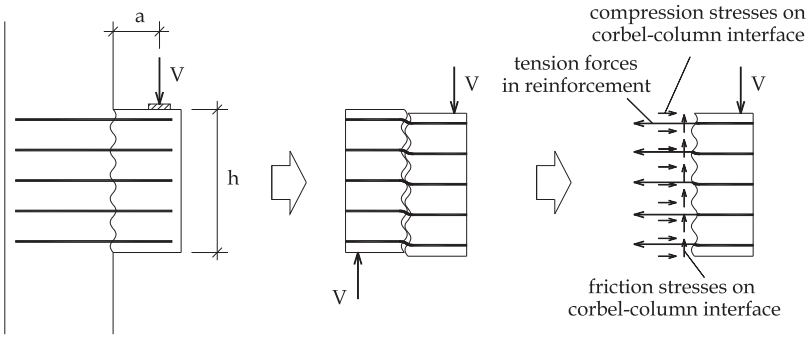

Fig. 11. Mechanism of resistance in the Shear-Friction Model for corbels.

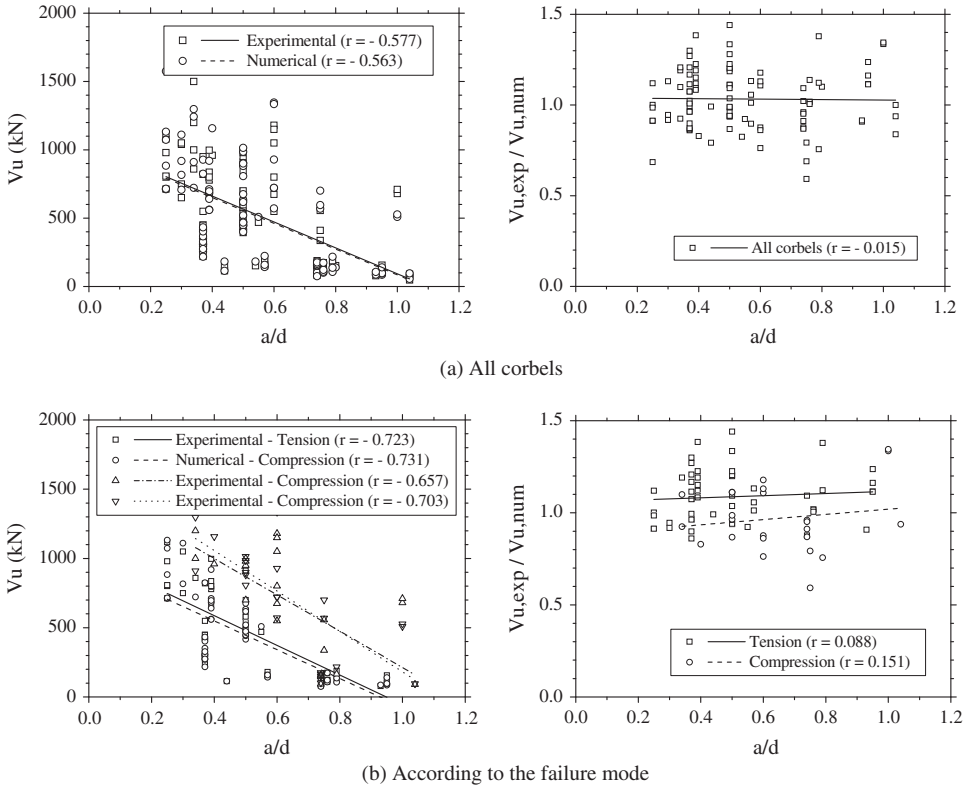

Fig. 12. Shear span-to-effective depth ratio (a/d) *versus* ultimate load (V_u).

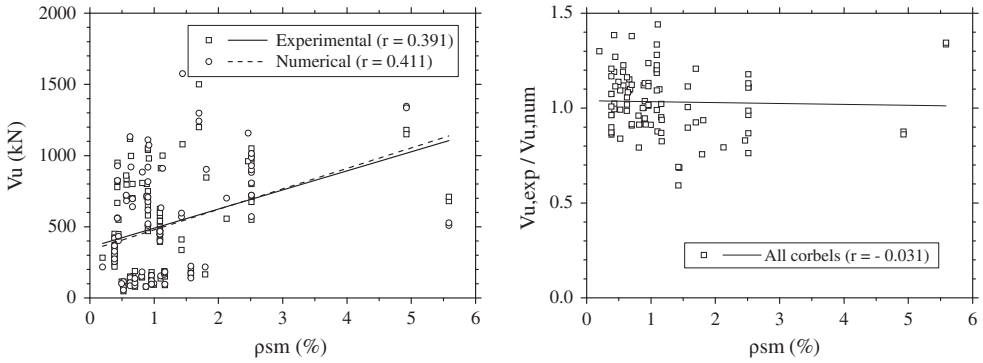

Fig. 13. Main reinforcement rate (ρ_{sm}) *versus* ultimate load (V_u).

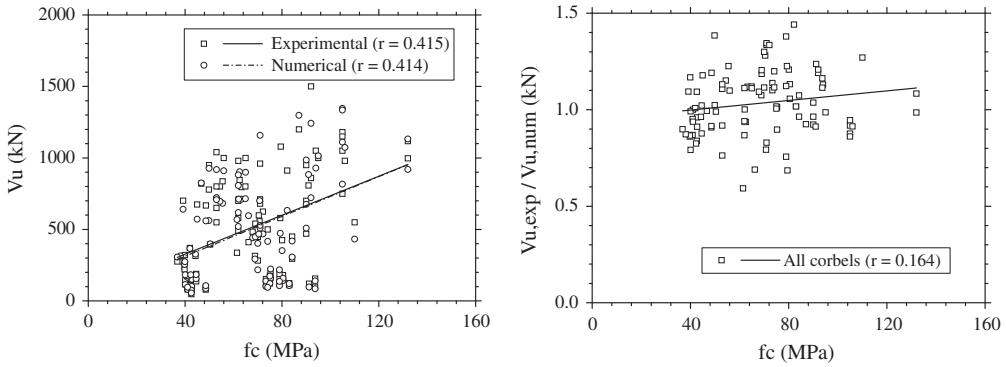

Fig. 14. Compressive strength of concrete (f_c) *versus* ultimate load (V_u).

Table 4
Contribution of the horizontal reinforcements of corbels that failed by tension.

Specimen	a/d	Demand level coefficients		Failure loads		
		γ'_{sm}	γ'_{shs}	$V_{u,exp}$ (kN)	Original numerical model with A_{shs}	Numerical model without A_{shs}
YO-B1	0.39	1.00	1.00	778	562	468
YO-B2	0.39	1.00	1.00	667	560	466
YO-C1	0.39	1.00	1.00	796	711	581
YO-C2	0.39	1.00	1.00	836	682	591
YO-D1	0.39	1.00	0.93	701	641	555
YO-D2	0.39	1.00	1.00	801	696	597
YO-E1	0.25	1.00	1.00	712	711	607
YO-E2	0.25	1.00	1.00	801	715	595
YO-E3	0.25	1.00	1.00	1079	1575	1371
YO-F1	0.50	1.00	1.00	912	633	519
YO-F2	0.50	1.00	0.83	845	903	770
YO-G2	0.75	0.94	0.70	411	596	529
FA-T8	0.74	0.97	0.36	188	184	148
FO-SC1-3	0.50	1.00	1.00	700	675	557
FO-SC2-3	0.50	1.00	0.99	580	618	521
FO-PF2	0.30	1.00	1.00	1050	1110	770
RE-C11	0.37	1.00	1.00	820	825	623
NA-SP5	0.37	1.00	1.00	275	315	271
NA-SP6	0.37	1.00	1.00	275	306	248
NA-SP10	0.37	1.00	1.00	450	419	293
NA-SP11	0.37	1.00	1.00	425	352	290
NA-SP13	0.37	1.00	1.00	315	327	279
NA-SP14	0.37	0.99	1.00	370	367	275
TO-CH5V5	0.50	1.00	0.91	625	468	440
TO-CH5V0	0.50	1.00	0.89	535	451	431
TO-CH4V4	0.50	1.00	0.98	540	448	439
TO-CH4V0	0.50	1.00	0.92	580	473	446
TO-CH6V0	0.50	0.98	0.73	598	467	430
TO-CH4V4*	0.50	1.00	0.78	395	399	373
FE-CS5-4A	0.57	1.00	1.00	150	142	98
FE-CD6-4A	0.57	1.00	1.00	180	159	114
FE-CS6-4A	0.57	1.00	1.00	160	158	115
FE-CS8-5A	0.57	1.00	1.00	200	223	175
FE-CD5-4B	0.76	1.00	1.00	110	108	74
FE-CD6-4B	0.76	1.00	1.00	124	122	89
FE-CS6-4B	0.76	1.00	1.00	123	121	88
FE-CS8-5B	0.76	1.00	0.98	175	174	138
FE-CS5-4C	0.95	1.00	0.95	100	86	63
FE-CD6-4C	0.95	1.00	0.93	106	95	75
FE-CS6-4C	0.95	1.00	0.96	120	97	75
FE-CS8-5C	0.95	1.00	0.87	156	140	111
BO-C1-80	0.37	1.00	1.00	282	217	168
BO-C2-80	0.37	1.00	1.00	448	402	319
BO-C3-80	0.25	1.00	0.98	807	884	614
BO-C1-100	0.25	1.00	0.96	980	1073	719
BO-C2-100	0.37	1.00	1.00	550	433	324
BO-C1-120	0.25	1.00	0.98	1117	1133	564
BO-C2-120	0.39	1.00	0.98	997	920	445
CA-MI-2ϕ10 + 4ϕ6	0.93	1.00	0.79	97	106	87
CA-MII-2ϕ10 + 4ϕ6	0.79	1.00	1.00	189	137	106
Average		1.00	0.95	Mean decrease of $V_{u,num}$ (%)		20.4
Standard deviation (%)		1.00	11.22			
Variation coefficient (%)		1.00	11.84			

as shown in Fig. 11. A frictional strength is mobilized due to the shear forces acting along the cracked plane with rough irregular faces. With the slippage along the crack, this irregular cracked plane causes the separation between the two elements, and the reinforcement is stressed. The tension forces in reinforcement are equilibrated by compression stresses on concrete interface, which mobilize friction stresses on this interface.

Some common aspects of these two mechanisms were observed for the corbels analyzed in this paper, as visualized in Figs. 7–9, such as: the sloping compression stresses and strains fields representing the diagonal strut of the Strut-and-Tie Model; the almost horizontal tensile strain field in the upper region of the corbel indicating the region necessary to be reinforced, representing the main tie of the Strut-and-Tie Model; tensile strains transverse to the sloping compression stresses and strains fields, indicating the spreading of these compression fields which represent the bottle-shaped strut of the corbels; the concentration of stress and strain near the plate and the lower corner of the corbel-column interface, representing the nodal regions of the Strut-and-Tie Model; an region almost free of stresses in the rectangular corbels, indicating an economy of material in chamfer shaped corbels; and a smeared cracking in the corbel-column interface, indicating the mobilization of Shear-Friction mechanism.

4.6. Influence of the main parameters in the failure load

The effect of the parameters such as the shear span-to-effective depth ratio (a/d), the main reinforcement rate (ρ_{sm}) and the compressive strength of concrete (f_c) could be evaluated through the numerical simulations and these ones were also compared to the experimental results.

The good agreement between the numerical and experimental results can be visualized through the ratio $V_{u,exp}/V_{u,num}$, which was around 1, *versus* the parameters a/d, ρ_{sm}, and f_c, showed, respectively, in Figs. 12–14.

Fig. 12(a) shows the influence of the shear span-to-effective depth ratio (a/d) in the experimental and numerical failure loads (V_u). Not only for experimental results but also for numerical results, larger the ratio a/d lower the failure load V_u. Comparing the linear correlation coefficients r of Pearson between the ratio a/d and the failure load V_u of each regression with the critical value for a sample size $n = 100$ and a significance level $A = 0.05$, there is a significant linear correlation between those parameters. The linear regression lines of the numerical simulation were very close to the experimental line, showing that the corbels behavior was well captured by ATENA. Separating the corbels that had their failure mode by tension or compression correctly predicted by the numerical analysis in Fig. 12(b), it is possible to note that the upper limit of capacity of the corbels is provided by the compression failure criterion.

The influence of other important parameters on the ultimate load (V_u), such as the main reinforcement rate (ρ_{sm}) and the compressive strength of concrete (f_c) can be visualized in Figs. 13 and 14, respectively. Both present a positive effect on the strength of corbels. The linear correlation coefficients r of Pearson between ρ_{sm} and V_u and between f_c and V_u compared to the critical value indicate that these parameters have a large linear correlation between each other. The numerical simulation had a fit very close to the experimental regression line.

4.7. Contribution of secondary reinforcements

Considering the good agreement with the experimental results, other aspects not well-explored in the tests, such as the improvement of the corbels behavior caused by the horizontal and vertical secondary reinforcements (A_{shs} and A_{svs}), could be better investigated by the numerical modeling. These secondary reinforcements have an important role in the improvement of cracks distribution of the corbels, in the confinement of the concrete region forming the diagonal strut, providing a certain ductility and, consequently, involving a less sudden failure. Considering these aspects, the secondary reinforcements are indispensable, primarily for reinforced high strength concrete corbels. In addition, the horizontal secondary reinforcement (A_{shs}) can potentially contribute to the resistant capacity of the corbels.

The demand level of the main, horizontal secondary and vertical secondary reinforcements can be evaluated, respectively, by Eqs. 1–3.

$$\gamma_{sm} = \frac{\sum(\sigma_{smi} \cdot A_{smi})}{f_{ym} \sum A_{smi}} \quad (1)$$

$$\gamma_{shs} = \frac{\sum(\sigma_{shsi} \cdot A_{shsi})}{f_{yhs} \sum A_{shsi}} \quad (2)$$

$$\gamma_{svs} = \frac{\sum(\sigma_{svsi} \cdot A_{svsi})}{f_{yvs} \sum A_{svsi}} \quad (3)$$

By Eq. (1), it is possible to analyze if all main rebars of the numerical model yielded ($\gamma_{sm} = 1$), or not ($\gamma_{sm} < 1$). This coefficient was calculated in order to measure the yielding degree of the main reinforcement of the numerical models for the corbels that experimentally failed by the yielding of this reinforcement.

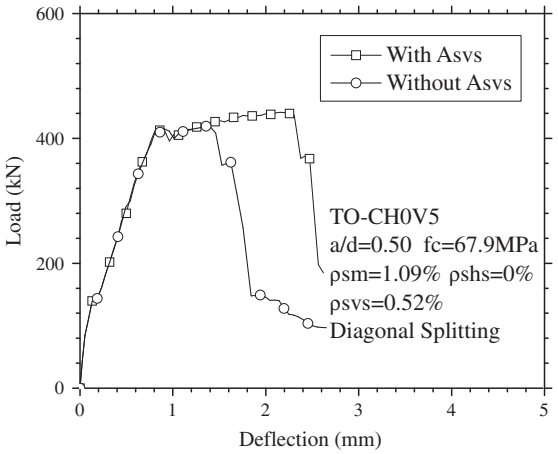

Fig. 15. Load–deflection response for the numerical model TO-CH0V5.

Table 5
Demand level coefficients (γ_{svs}) of the vertical secondary reinforcement.

Specimen	a/d	Demand level coefficient γ_{svs}
TO-CH5V5	0.50	0.12
TO-CH0V5	0.50	0.52
TO-CH4V4	0.50	0.13
TO-CH4V4*	0.50	0.45
FE-CS5-4A	0.57	0.12
FE-CD6-4A	0.57	0.08
FE-CS6-4A	0.57	0.11
FE-CS8-5A	0.57	0.19
FE-CD5-4B	0.76	0.27
FE-CD6-4B	0.76	0.26
FE-CS6-4B	0.76	0.26
FE-CS8-5B	0.76	0.39
FE-CS5-4C	0.95	0.29
FE-CD6-4C	0.95	0.36
FE-CS6-4C	0.95	0.33
FE-CS8-5C	0.95	0.50
Average		0.27
Standard deviation (%)		14.25
Variation coefficient (%)		52.28

Table 4 shows the coefficient γ_{sm} referred to the main reinforcement and, γ_{shs} to the horizontal secondary reinforcement, for the corbels that experimentally failed by the yielding of the main reinforcement. According to the γ_{sm} values shown in Table 4, only for few corbels, those that had some parameter adopted or approached, the main reinforcement of the numerical models did not completely yield. There was a significant demand of the horizontal secondary reinforcement in the numerical models, expressed by γ_{shs} mean value around 0.95 for the medium and coarse meshes, which better represented the corbels that failed by tension.

The role of the horizontal secondary reinforcement in the corbel strength could be also evaluated through the numerical analysis of the corbels removing this referred reinforcement. Table 4 shows that there was a decrease in the ultimate load for the numerical models without the horizontal secondary stirrups. The mean decrease of the ultimate load was around 20%. For some corbels with low a/d ratio, the percentile decrease in function of the removal of the horizontal secondary reinforcement (A_{shs}) reached more than 50%, and for other corbels with larger a/d up to 30%. Therefore, the horizontal secondary reinforcement (A_{shs}) significantly improves the load capacity of high strength concrete corbels and can be considered in the design models.

The role of the vertical secondary reinforcement can be visualized through Fig. 15 and Table 5. Table 5 shows the demand level coefficients (γ_{svs}) of the vertical secondary reinforcement. The mean coefficient was rather low, with the mean value equal to 0.27, indicating that these vertical stirrups only effectively contribute to the improvement of the cracking distribution and the ductility. In order to analyze these aspects, the corbel TO-CH0V5 of Torres [22], with secondary reinforcement only in the vertical direction, was reprocessed without the vertical stirrups. Fig. 15 clearly shows that the absence of this reinforcement decreases the ductility of the corbel.

5. Conclusions

This paper aimed at investigating the behavior of reinforced high strength corbels. For this analysis, the software ATENA was selected for the analysis and the obtained results were compared to the experimental results of one hundred corbels available in the technical literature.

In order to investigate possible different results due to the smeared approach used, some preliminary numerical simulations with three meshes sizes, named of fine, medium and coarse meshes, were evaluated. These preliminary models showed that the mesh size did not significantly affect the results, confirming the smeared approach and the reduction of the element size and element orientation effects used in ATENA. But for avoiding an excessive computational effort and loss of precision in characterization of the cracking pattern, the other numerical simulations were done with the medium mesh size.

ATENA provided a good prediction of the experimental failure mode by tension or by compression for almost all corbels. For the corbels with a more complete characterization, the failure mode of the numerical models was more close to the actual one.

The load efficiency factor was close to one, with the average factor larger than one, which is the desirable value for a safe analysis. Analyzing the coefficient of determination, which indicates how closely values obtained from fitting models match the experimental results, the numerical simulation provided a very good prediction of the experimental failure load.

Analyzing the linear fit curves, there is a strong linear correlation of the failure load (V_u) with important parameters such as the shear span-to-effective depth ratio (a/d), the main reinforcement rate (ρ_{sm}) and the compressive strength of concrete (f_c). The inverse proportional ratio between V_u and a/d was observed, and a direct one between V_u and the other two parameters (ρ_{sm} and f_c). The numerical linear fit curves were also compared to the experimental results.

Regarding the load–deflection and load-stress at reinforcement responses, the numerical results were reasonably close to the experimental curves. Also, the cracking, stress and strain fields were well characterized by the numerical simulations and could be associated to the two mechanisms that govern the corbel behavior, originated by the Strut-and-Tie and Shear-Friction Models.

Considering the good agreement with the experimental results, this numerical analysis also allowed evaluating the role of the secondary reinforcements for the behavior of corbels. As mentioned in technical literature and proved in the numerical models, the horizontal secondary reinforcement improves the load capacity of the corbels and other properties as cracking distribution and ductility. On the other hand, the vertical secondary reinforcement does not increase the strength of the corbels, but contributes for the improvement of the cracking distribution and ductility. Therefore, the horizontal and vertical secondary reinforcements are indispensable to reinforced high strength concrete corbels. However, only the horizontal secondary reinforcement could be considered in the capacity strength of the corbels.

Acknowledgements

The authors would like to acknowledge the Brazilian government agency CAPES, for the Post-Doctoral scholarship of the first author, the University of Illinois at Urbana-Champaign by the support for the Post-Doctoral stage of the first and fourth authors, and CNPq and FAPITEC, for the financial support. The conclusions and opinions expressed in this paper are the authors' responsibility and do not reflect the points of view of the sponsors.

Appendix A. Supplementary material

Supplementary data associated with this article can be found, in the online version, at http://dx.doi.org/10.1016/j.engstruct.2014.05.014.

References

[1] Schlaich J, Schafer K, Jennewein M. Toward a consistent design of reinforced concrete structures. J Prestressed Concr Struct 1987;32(3):74–150.
[2] ACI (American Concrete Institute) ACI Committee 318/08 - Building Code Requirements for Structural Concrete (ACI 318-08) and Commentary (ACI 318R-08). Michigan, Farmington Hills; 2008. 471pp.
[3] PCI (Precast/Prestressed Concrete Institute) PCI Design Handbook – Precast and Prestressed Concrete. 7th ed. Chicago, IL: PCI; 2010.
[4] European Committee Standardization. Eurocode 2 – Design of concrete structures – Part 1-1: General rules and rules for buildings. London: BSI; 2004. 230p.
[5] Strauss A, Mordini A, Bergmeister K. Nonlinear finite element analysis of reinforced concrete corbels at both deterministic and probabilistic levels. Comput Concr 2006;3(2/3):123–44.
[6] Gao D, Zhang J. Finite element analysis of shear behaviors for steel fiber reinforced concrete corbels by ANSYS. Proceedings of the 2010 second international conference on computer modeling and simulation (ICCMS '10). vol. 4; 2010. p. 303–7.
[7] Souza RA. Experimental and Numerical Analysis of Reinforced Concrete Corbels Strengthened with Fiber Reinforced Polymers. Proceedings of Computational Modelling of Concrete Structures – EURO C10; 2010. Schladming.
[8] Rezaei M, Osman SA, Shanmugam NE. Finite element analysis of reinforced concrete corbels. Proceedings of 3' WSEAS International Conference on Engineering Mechanics, Structures, Engineering Geology – EMESEG '10; 2010. p. 448–52.
[9] Syroka E, Bobiński J, Tejchman J. FE analysis of reinforced concrete corbels with enhanced continuum model. Finite Elem Anal Des 2011;47(9):1066–78. Sept.
[10] Yong YK, McCloskey DH, Nawy EG. Reinforced corbels of high-strength concrete. In: ACI SP-87. High-strength concrete. Detroit (Michigan): ACI; 1985. p. 197–212.
[11] Yong YK, Balaguru P. Behavior of reinforced high-strength concrete corbels. J Struct Eng 1994;120(4):1182–201. Jan/Feb.
[12] Fattuhi NI, Hughes BP. Reinforced steel an polypropylene fiber concrete corbel tests. Struct Eng 1989;67(4):68–72.
[13] Fattuhi NI, Hughes BP. Reinforced steel fiber concrete corbels with various shear span-to-depth ratios. ACI Mater J 1989;86(6):590–6. Nov/Dec.
[14] Fattuhi NI, Hughes BP. Ductility of reinforced concrete corbels containing either steel fibers or stirrups. ACI Struct J 1989;86(6):644–51. Nov/Dec.
[15] Fattuhi NI. Reinforced concrete corbels made with high-strength concrete and various secondary reinforcements. ACI Struct J 1994;91(4):376–83. Jul/Aug.
[16] Selim HS, Foster SJ, Gowripalan N. Experimental Investigation on High-Strength Concrete Corbels. UNICIV Report No. R-310, University of New South Wales, School of Civil Engineering; 1993. 146 p. Jan.
[17] Powell RE, Foster SJ. Experimental Investigation on Rectangular Corbels Cast in High-Strength Concrete. UNICIV Report No. R-338, University of New South Wales, School of Civil Engineering; 1994. 216 p. Aug.
[18] Foster SJ, Powel RE, Selim HS. Performance of high-strength concrete corbels. ACI Struct J 1996;93(5):555–63. Sept-Oct.
[19] Reis APA, Torres FM. Experimental analysis of reinforced concrete corbels. Final Project of Undergraduate Course, Goiânia, Federal University of Goiáis, School of Civil Engineering; 1996. 106p [in Portuguese: Estudo experimental de consolos em concreto armado].
[20] Torres FM, Reis APA, Gomes RB, Andrade MAS, Pinheiro LM. Estudo teórico-experimental da força de ruína de consolos. Proceedings of 28th Jornadas Sul-Americanas de Engenharia Estrutural. vol. 3. São Carlos, SP: EESC-USP; 1997. p. 1005–14.
[21] Naegeli CH. Analysis of reinforced concrete corbels. Rio de Janeiro. 224p. Ph.D. thesis. Pontifícia Universidade Católica do Rio de Janeiro; 1997 [in Portuguese: Estudo de consolos de concreto armado).
[22] Torres FM. Theoretical-experimental analysis of reinforced concrete corbels. 95p. M.S. thesis. Escola de Engenharia de São Carlos, Universidade de São

Paulo; 1998 [in Portuguese: Análise teórico-experimental de consolos de concreto armado].
[23] Fernandes GB. Behavior of reinforced high-strength concrete corbels – experimental Investigation and Design Model. Proceedings of '2 CANMET/ACI international conference on high-performance concrete and performance and quality of concrete structures. Gramado: Farmington Hills, ACI; 1999. pp. 445–62.
[24] Bourget M, Delmas Y, Toutlemond F. Experimental study of the behavior of reinforced high-strength concrete short corbels. Mater Struct 2001;34:155–62. April.
[25] Campione G, La Mendola L, Papia M. Flexural behaviour of concrete corbels containing steel fibers or wrapped with FRP sheets. Mater Struct 2005;38:617–25. July.
[26] Campione G, La Mendola L, Mangiavillano ML. Steel fiber-reinforced concrete corbels: experimental behavior and shear strength prediction. ACI Struct J 2007;104(5):570–9. Sept-Oct.
[27] Cervenka V, Cervenka J. ATENA Program Documentation – Part 2-1: User's Manual for ATENA2D. Prague; 2003.
[28] Cervenka V, Cervenka J. ATENA Program Documentation – Part 2-2: User's Manual for ATENA3D. Prague; 2005.
[29] Bazant ZP, Oh BH. Crack band theory for fracture of concrete. Matériaux et Constructions 1983;16(93):155–77.
[30] Rots JG, Nauta P, Kusters GMA, Blaauwendraad J. Smeared crack approach and fracture localization in concrete. Heron 1985;30(1):1–48. Delft, Netherlands.
[31] Feenstra PH, Borst R. Aspects of robust computational modeling for plain and reinforced concrete. Heron 1993;38(4):3–76. Delft, Netherlands.
[32] ACI (American Concrete Institute) ACI Committee 363/93 – State-of-the-Art Report on High-Strength Concrete. ACI Manual of Concrete Practice, v. 1. Detroit, American Concrete Institute; 1993 and later editions. 363R-1-363R-55.
[33] Vecchio FJ, Collins MP. Response of Reinforced Concrete to In-Plane Shear and Normal Stresses. Publication No. 82-03, Department of Civil Engineering, University of Toronto; 1982. 332 p. Mar.
[34] Thorenfeldt E, Tomaszewicz A, Jensen JJ. Mechanical Properties of High Strength Concrete and Application to Design. Proceedings of the Symposium Utilization of High-Strength Concrete. Stavanger, Norway, Tapir, Trondheim; 1987. p. 149–59. June.
[35] Mattock AH, Chen KC, Soonswang K. The behavior of reinforced concrete corbels. PCI J 1976;21(3):18–42. May–June.
[36] Fattuhi NI. Column-load effect on reinforced concrete corbels. J Struct Eng 1990;116(1):188–97. Jan.
[37] Hagberg T. Design of concrete brackets: on the application of the truss analogy. ACI J 1983;80(1):3–12. Jan–Feb.
[38] Kriz LB, Raths CH. Connections in precast concrete structures – strength of corbels. PCI J 1965;10(1):16–61.
[39] Somerville G. The behaviour and design of reinforced concrete corbels. In: ACI SP-42. Shear in reinforced concrete. Detroit: ACI; 1974. p. 477–502.
[40] Leonhardt F, Mönnig E. Vorlesungen uber Massivbau. Berlin: Springer-Verlag; 1973. (Portuguese version: Construções de concreto: Casos especiais de dimensionamento de estruturas de concreto armado. vol. 2, 1.ed. Rio de Janeiro, Interciência; 1977).